The carbon dioxide solubility in alkali basalts: an experimental study

Priscille Lesne, Bruno Scaillet, Michel Pichavant, Jean-Michel Bény

The carbon dioxide solubility in alkali basalts: an experimental study

Priscille LESNE [1,*], Bruno SCAILLET [1], Michel PICHAVANT[1], Jean-Michel BENY[1]

[1]CNRS/INSU-Université d'Orléans-Université François Rabelais Tours, UMR 6113, Institut des Sciences de la Terre d'Orléans, 1A, rue de la Férollerie, 45071 Orléans Cedex 02, France

*Corresponding author:

e-mail: P.Lesne@bristol.ac.uk

present address: Department of Earth Sciences, University of Bristol, Wills Memorial Building, Queens Road, Bristol, BS8 1RJ, U.K.

Abstract:

Experiments were conducted to determine CO_2 solubilities in alkali basalts from Vesuvius, Etna and Stromboli. The basaltic melts were equilibrated with nearly pure CO_2 at 1200°C under oxidizing conditions, and at pressures ranging from 269 to 2060 bars. CO_2 solubility was determined by FTIR measurements. The results show that alkalis have a strong effect on the CO_2 solubility and confirm and refine the relationship between the compositional parameter Π devised by Dixon (1997) and the CO_2 solubility. A general thermodynamic model for CO_2 solubility in basaltic melts is defined for pressures up to 2 kbars. The new CO_2 solubility model yields saturation pressures lower by as much as 50% relative to existing models when applied to volatile-rich alkali basalts.

Key words: CO_2 solubility, alkali basalts, experiments, thermodynamics

Introduction

Dissolved volatiles in silicate melts dramatically influence the physical properties of magmas, such as density, viscosity, vesiculation, and largely control eruptive styles. Volatiles exsolve from melts into bubbles as magmas rise toward the earth's surface and depressurize (e.g., Blank et al., 1993). Such a process may give rise to explosive eruptions, leading to important human and material damages, and may have a major impact on the global Earth climate (Robock 2000). Water is generally the most abundant volatile in terrestrial magmas, CO_2 being the second most common species, notably in mafic compositions. Thus, understanding the thermodynamics of CO_2 in silicate melts can provide important constraints on the behaviour of basaltic reservoirs, the ensuing eruptive processes, and ultimately on the evolution of planetary degassing. To model basalt degassing during volcanic eruptions, a detailed knowledge of the mixing properties of volatile components in both fluid and melt is required since, because of its low solubility, carbon dioxide is usually a major component of the gases escaping from magmas as they rise through the crust.

Experiments on CO_2 solubility in basaltic melts have been performed mostly at high pressures where dissolved CO_2 contents may reach several wt% (>10 kbar, Blank and Brooker, 1994, Morizet et al., 2002). At lower pressures, efforts have mainly focused on silicic liquids and only a few studies have been performed on CO_2 solubility in basaltic melts (e.g., Pawley et al., 1992, Dixon et al., 1995, Jendrzejewki et al., 1997; Behrens et al., 2009). As pointed out by Stolper and Holloway (1988), this gap of knowledge reflects in part the small influence of CO_2 on solid-liquid phase equilibria at low pressures, due to its low solubility in most silicate melts under such conditions. Another reason is the technical difficulties associated with the need to work at the high temperature conditions required for mafic compositions (e.g., Berndt et al., 2002; Di Carlo et al., 2006; Behrens et al., 2009), in particular in the mid pressure range (2-6 kbar) where solid pressure media, such as piston cylinders, are not routinely operated. More specifically, the low viscosity of mafic melts requires them to be fast quenched to prevent their crystallisation during cooling. This demands the implementation of appropriate experimental designs in gas pressure vessels (Holloway et al., 1992; Roux and Lefevre, 1992) and, for H_2O-bearing basalts, such devices may still fail to properly quench liquids to glasses (e.g., Behrens et al., 2009). As a consequence of these technical difficulties, the number of high quality solubility data in the low to mid pressure range has remained limited. In particular, alkali basalt compositions have received limited attention. Petrological studies indicate, however, that such alkali-rich compositions are volatile-rich, in particular in arc

settings (Dixon et al., 1997; Métrich et al., 2001; Bertagnini et al., 2004). Experimental data show indeed that alkali-rich basalt compositions tend to dissolve more CO_2 than those alkali-poor (Dixon, 1997; Botcharnikov et al., 2005; Behrens et al, 2009), a key role being played by potassium (Behrens et al., 2009) but the exact compositional control of such an increase is still unclear.

In an effort to decipher the role of alkalis on CO_2 solubility, in this study we report measurements of CO_2 solubility obtained in several basalts of varying alkalinity coming from Italian active volcanoes at 1200°C, at pressures ranging from 250 up to 2000 bar, and under oxidizing conditions. CO_2 contents in quenched glasses from vapour-saturated experiments were measured by infrared spectroscopy. Solubility measurements give upper bounds on the amounts of CO_2 that can dissolve in magmas at various temperatures and pressures. A companion paper presents the thermodynamics of water in these silicate melts. Our aim is to produce a set of internally consistent data on the solubility of C-O-H-S volatiles under moderately oxidizing conditions so as to be ultimately able to quantitatively model the degassing of alkali basalts, such as recently done for silicic compositions by Burgisser and Scaillet (2007).

Experimental techniques

Starting materials, capsules and charges

Three alkali basalts from Vesuvius, Etna and Stromboli (Lesne et al. this issue) were selected for our investigation. The natural samples were powdered and melted in a Pt crucible at atmospheric pressure, at 1400°C during 3 hours in order to get homogeneous and nominally anhydrous glasses. The resulting glasses were analyzed by electron microprobe. Their compositions are listed in Table 1. Experiments were conducted in parallel on those three alkali basalts.

As for experiments on water solubility, small glass chips were loaded in capsules to prevent bubble formation. About 60 to 100 mg of starting material was used for each experiment. Capsules (2 cm height, 2.5 mm inner and 2.9 mm outer diameters) made of platinum were used. CO_2 was added as silver oxalate ($Ag_2C_2O_4$, density 5g/cm^3). Although silver does dissolve in basaltic melt, its effect on CO_2 solubility has been shown to be negligible (Pan et al., 1991). Capsules were sealed by electric arc. They sere then put in an oven for several hours and reweighed to check for leaks.

Equipment and experiments

Equilibrium experiments between a fluid (CO_2-rich fluids, see below) and a silicate liquid phase were conducted in an internally heated pressure vessel (IHPV) operated in a vertical position and equipped with a drop quench set up (see Di Carlo et al., 2006). Experiments were performed at 1200±5°C, at the following pressures: 269, 524, 1013, 1062, 1128, 2059 ±25 bars, under oxidizing conditions. Experiments lasted between 4 to 8 hours. Based on previous experimental works performed using similar procedures, the equilibrium between the basaltic liquid and the fluid phase is considered to be reached under these conditions (e.g., Dixon et al, 1995; Botcharknikov et al, 2005; Behrens et al., 2009). Phase equilibrium experiments performed with the same duration and P-T-H_2O-CO_2 conditions (Di Carlo et al., 2006; Pichavant et al. 2009) on a Strombolian basalt had no problem in attaining crystal-liquid equilibrium. Since the kinetics of melt-fluid equilibrium is faster than that of crystal-liquid one, we conclude that our run durations were long enough to attain equilibrium. In support of this, major element analyses performed on two or three glass ships on microprobe yielded the same results within analytical error. The same was observed with FTIR analyses carried out on several double polished glass pieces (2 to 3).

Any use of sensor was not possible because of the short duration of the experiments. All the runs were done using the intrinsic fH_2 of the vessel, as measured by Pichavant et al. (2009) for experiments done with the same apparatus, without hydrogen added, at 1150°C, at 2010 and 880 bars (runs 22 and 23). We assume that the fH_2 measured in those experiments is equivalent to the fH_2 in our runs, then the fO_2 of each charge was calculated from the dissociation reaction of water, using fH_2O as calculated from the dissolved water content in the glass (see below). It appears that the fO_2 calculated for all charges, averages at NNO+1.9, with an error of 0.6 log unit. All performed experiments for this study are reported in Table 2.

Analytical techniques

Analytical techniques used in this study are the same as those used in the accompanying paper (Lesne et al.). Major elements were analysed with a SX50 CAMECA electron microprobe (BRGM-ISTO, Orléans, France). Water contents and its speciation were determined with FTIR analyses. All of these methods are described in detail in Lesne et al. (this issue). The total carbon dissolved in quenched glasses was determined by using transmission IR spectroscopy on doubly polished glass chips, with thicknesses varying between 60 and 270 µm. One sample (4#4) had very low CO_2 contents, which required the use of a thick double polished glass (370 µm).. Sample thicknesses were measured using an optical microscope to

within 3 μm. To determine the total carbon dissolved in the glass, a microchamber attachment to the FTIR Nicolet[TM] Magna Spectrometer 760 together with a white source, a KBr beamsplitter and a MCT-A detector (mercury, cadmium tellurium) were used. Analytical conditions for each analysis were 128 scans and a 2 cm^{-1} resolution. The diameter of the analyzed spot was 100 μm. The background was acquired in air at each measurement. For each sample, a minimum of 2 spots were made, in order to check the homogeneity of the sample.

Carbon can be dissolved in silicate melts either as molecular CO_2 or as carbonate groups CO_3^{2-} (e.g., Fine and Stolper, 1985, 1986, Morizet et al., 2002). The intensity of the 2350 cm-1 is attributed to the ν_3 antisymmetric stretch of molecular CO_2 (Fine and Stolper, 1985; Fine and Stolper, 1986). The peaks at 1515 cm^{-1} and 1435 cm^{-1} correspond to an antisymmetric stretch of distorted CO_3^{2-} groups (Fine and Stolper, 1986). Figure 1 shows a typical IR spectrum obtained on our glasses which shows that there is a double peak at 1515 cm-1 and 1435 cm-1, whilst none is present at 2350 cm^{-1}. Thus, the carbon dissolved in the melt is present as carbonate groups (CO_3^{2-}) only, in agreement with previous works on basaltic compositions (e.g., Pan et al., 1991; Behrens et al., 2009).

In this work, following Behrens et al. (2009), we measured carbonate absorbance by substracting from the sample spectrum that of a compositionally similar but volatile-free glass (ie the starting dry glass) scaled to the same thickness of the unknown. This enables to model the background and measure the peak height of the 1515 cm^{-1} wavenumber.

The total carbon content of glasses was calculated with the Beer-Lambert law (Fine and Stolper 1985;1986), by measuring the absorbance of the 1515 cm^{-1} band:

$$C_{CO_2} = \frac{A_{1515} * M_{CO_2}}{d * \rho * \varepsilon_{1515}} \qquad (1)$$

Where C_{CO_2} is the total carbon content in the glass (in wt%), A_{1515} is the absorbance of the 1515 cm^{-1} band, d is the thickness of the sample (in cm), ρ is the density in g.l^{-1}, ε_{1515} is the molar extinction coefficient (l.mol^{-1}.cm^{-1}), and M_{CO_2} is the molecular weight of CO_2.

Glass densities, were calculated using the method of Richet et al. (2000), considering only the amount of water dissolved in the glass, assuming that the small quantities of CO_2 dissolved do not affect density to any measurable extent (Lange, 1994, Bourgue and Richet, 2001).

The choice of appropriate molar extinction coefficients is crucial to measure correctly dissolved carbon contents (e.g. Behrens et al., 2009). However, we do not have bulk carbon data, and thus it is not possible to obtain molar extinction coefficients for each basaltic

compositions studied here. Consequently, two choices are offered: either we arbitrarily take the same value for the three basaltic compositions, referring to Fine and Stolper (1986) (ε_{1515} =375±20 l.mol^{-1}.cm^{-1}, calculated for basaltic glasses), or we calculate the extinction coefficient for each basaltic melt using the method of Dixon and Pan (1995). These authors found a linear dependency of the molar extinction coefficient with the Na/(Na+Ca) molar ratio, in the range 0.25 to 0.5. Values of molar extinction coefficients determined by Dixon and Pan's method yield 381 l.mol^{-1}.cm^{-1} for Vesuvius, 327 l.mol^{-1}.cm^{-1} for Etna and 367 l.mol^{-1}.cm^{-1} for Stromboli samples. The calculated extinction coefficients for both Vesuvius and Stromboli are within 2% of the Fine and Stolper (1986) value, whilst that for Etna is lower by 13%, which reflects its higher Na content.. Behrens et al. (2009) determined the extinction coefficient of their phonotephrite melt to be 308±110 l.mol^{-1}.cm^{-1}, whilst the value retrieved with the Dixon and Pan (1995) method is 370 l.mol^{-1}.cm^{-1}. Although both values agree within error, the difference observed suggests that the Dixon and Pan method may overestimate extinction coefficients of strongly potassic compositions by up to 20%, which translates into a similar overestimates of carbon contents calculated with the Beert-Lambert law. In the following, owing to the lack of absolute method to measure dissolved C content, and considering the significant errors associated to existing measurements of extinction coefficients for basaltic compositions, we first present the results obtained by using the same extinction coefficient for all compositions, and latter discuss the effect arising from the use of composition specific molar extinction coefficients .

In addition to the uncertainty on extinction coefficients, one of the largest sources of errors in measuring the total carbon dissolved in the melt by FTIR arises from the method chosen to model the background. The method used here is somewhat subjective and leads to an error in absorbance estimated to be ±0.015, which propagates into an error of ± 50 ppm of the CO_2 dissolved in the glass, regardless of the CO_2 contents. Thicknesses were measured to within 3 μm which induces an error of 2% on the total CO_2 contents dissolved in the melt. The maximum error on the density calculations is equal to 20%. Altogether we estimate that the CO_2 content reported in this work are known to within 20%.

Results

The fluid-saturated charges have been checked after each experiment: capsules were first weighed to check any volatile loss during experiment, then they were punctured. Any escape of bubbles/gas and difference of weigh between before and after piercing is a proof of fluid-saturated experiment. All the data presented in this study are fluid saturated.

Macro and microscopic observations

Run products were translucent to brownish glasses, becoming darker and opaque when quench crystals (<5μm) were present (i.e., in experiments performed with more than 4 capsules). Most quenched glasses contain a few microbubbles whose abundance does not exceed 0.1 % in volume. Larger bubbles (<0.5mm of diameter), indicative of fluid saturation at P and T, are located at the melt/capsule interface, as shown by the presence of large open smooth cavities at the surface of the glass blocks.

Major elements and H_2O contents

The compositions of quenched glasses are reported in the Table 3. Analytical errors were less than 0.2% for all oxides, except for SiO_2 (0.4 to 0.6%) and for Fe_{tot} (less than 0.4%). Apart from Fe_{tot}, the concentrations of major oxides do not differ appreciably from those of the starting materials (Table 1).

For experiments carried out in platinum capsules, the iron loss is around 30%, whereas the iron loss of experiments carried out in $Au_{75}Pd_{25}$ capsules is less than 10% (Table 3).

Despite that no water was added to the capsules, the water contents of quenched glasses vary between 0.70 and 1.30 wt% without any obvious relationships with pressure or melt composition. Several sources of water can be proposed: it could come from the silver oxalate which contains some water (up to 5 wt%) and could not be dried enough, or from adsorption of atmospheric water on the starting glasses. However, the most probable source of H_2O is from reduction of ferric into ferrous iron (e.g., Holloway et al., 1992), inasmuch as our starting glasses are oxidized, which enables the operation of the following reaction:

$$Fe_2O_3 + H_2 \Leftrightarrow FeO + H_2O \ (2).$$
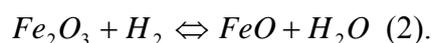
Note that, in addition to the above reaction, reduction of ferrous iron via alloying with the capsule wall will also produce some water.

CO_2 contents

Dissolved CO_2 contents in glasses are reported in Table 3. We stress that, as the quenched glasses also contain dissolved H_2O, the measured CO_2 contents do not represent pure CO_2 solubilities. The data show linear relationships between dissolved carbon and pressure for each composition (figure 2). Data from Dixon et al. (1995) and Behrens et al. (2009) are also shown for comparison. Figure 2 shows clearly that there is a strong dependence of the carbon dissolved in the melt on melt composition. Alkali-rich compositions dissolve more CO_2 than

7

those alkali-poor. However, to rigorously compare CO_2 solubilities of the different melt compositions, one has to determine the fugacities of CO_2.

Determination of the fugacities of CO_2.

As the H_2O of quenched glasses was determined in each charge, and as solubilities laws of water were defined for each composition in the companion paper (Lesne et al.), we can calculate the f_{H_2O} of each charge, using the following empirical relationships derived from the experimental data base of Lesne et al. (this issue):

$$f_{H_2O}^{1200°C} = 126.54 \times (wt\%H_2O)^{1.69} \qquad \text{for Vesuvius} \qquad (3);$$

$$f_{H_2O}^{1200°C} = 104.98 \times (wt\%H_2O)^{1.83} \qquad \text{for Etna;} \qquad (4);$$

$$f_{H_2O}^{1200°C} = 128.49 \times (wt\%H_2O)^{1.73} \qquad \text{for Stromboli.} \qquad (5).$$

In the above equations $wt\%H_2O$ is the wt% amount of total water dissolved in the quenched glasses. Once the f_{H_2O} is known, we can derive the mole fraction of H_2O ($X_{H_2O}^f$) in the coexisting fluid by using the standard relationships:

$$f_i = \gamma_i * P_i \ (6),$$

where γ_i is the fugacity coefficient of species i, and P_i its partial pressure.

Since

$$P_i = X_i * P_{tot} \ (7), \text{ where } P_{tot} \text{ is total pressure,}$$

we obtain

$$f_i = \gamma_i * X_i * P_{tot} \ (8).$$

Assuming that the fluid is made of only H_2O and CO_2 species (under oxidized conditions CO_2 has been shown to be the only C-bearing species in the C-O-H system, Pawley et al., 1992), it follows:

$$X_{H_2O} + X_{CO_2} = 1 \ (9),$$

and so

$$X_{CO_2} = 1 - X_{H_2O} \ (10).$$

In this work, we use the γ_{CO_2} and γ_{H_2O} values of Dixon et al. (1995). These fugacity coefficients correspond to those of pure species at P and T. Strictly speaking, the fugacity coefficient of any species i in a complex fluid is dependent on the composition of that fluid, in addition to P and T, and this can be accounted for via the use of a modified Redlich Kwong equation of state with appropriate mixing rules between different fluid species (Holloway,

1987; Ferry and Baumgartner, 1987). However, in the low pressure and high temperature range of interest here, application of the rules of real mixing of real fluid has only a trivial effect on the calculated fugacity coefficients (less than 1 %, see Holloway, 1977), relative to the assumption of ideal mixing of real fluids (Lewis and Randall rule) which has thus been used here for simplicity. Application of the empirical relationships 2-4 assumes also that dissolved CO_2 does not affect the thermodynamics of H_2O solution in the selected melts. Considering the low concentration in CO_2 of our synthetic melts, this assumption holds true to a first approximation. The reverse (ie H_2O affects the CO_2 solubility) might not be true, however, as discussed below. Using such an approach, the fugacity of CO_2 of any run product can be calculated in a way that ensures internal consistency between fluid species fugacities:

$$f_{CO_2} = \gamma_{CO_2} \times X_{CO_2} \times P_{tot} \ (11).$$

The relationships between dissolved CO_2 ($X_{CO_2}^m$ being the mole fraction of CO_2 dissolved calculated following Silver and Stolper (1985) on the basis of one oxygen) and f_{CO_2} are shown in figure 3.

Each trend can be fitted to a second order polynomial equation, in mole fractions:

$$f_{CO_2}^{1200°C} = 8.57 \times 10^6 \times X_{CO_2}^{m \ 1.26}; \qquad R^2 = 0.99 \text{ for Vesuvius} \qquad (12)$$

$$f_{CO_2}^{1200°C} = 1.14 \times 10^7 \times X_{CO_2}^{m \ 1.23}; \qquad R^2 = 0.93 \text{ for Etna} \qquad (13)$$

$$f_{CO_2}^{1200°C} = 3.49 \times 10^6 \times X_{CO_2}^{m \ 1.04}; \qquad R^2 = 0.99 \text{ for Stromboli} \qquad (14)$$

or in ppm:

$$f_{CO_2}^{1200°C} = 1.93 \times 10^{-1} \times CO_2^{melt \ 1.26}; \qquad R^2 = 0.99 \text{ for Vesuvius} \qquad (15)$$

$$f_{CO_2}^{1200°C} = 4.06 \times 10^{-1} \times CO_2^{melt \ 1.22}; \qquad R^2 = 0.93 \text{ for Etna} \qquad (16)$$

$$f_{CO_2}^{1200°C} = 1.62 \times CO_2^{melt \ 1.04}; \qquad R^2 = 0.99 \text{ for Stromboli} \qquad (17)$$

f_{CO_2} versus co_2^{melt} relationships for MORB (Dixon et al., 1995) is also shown on figure 3: the CO_2 solubility varies non-linearly with fluid composition. Again, the dependence of the total dissolved carbon with melt composition is apparent. It should be stressed that equations 12-17 are essentially valid for the selected melt compositions having dissolved water contents similar to those of the present work and over the pressure range investigated (1-2 wt% and up to 2 kb). On figure 3 we have also plotted the data of Behrens et al (2009), calculating the fCO$_2$ using their measured XCO$_2$ and equation (11). Despite some scatter, in part related to

quench effects arising from the excessively low viscosity of phonotephrite melt, the data display a similar exponential pattern, being located to the right of the Vesuvius trend, which is in keeping with the much stronger potassic character of the phonotephrite composition (7.52 wt% K_2O) used by Behrens et al. (2009) relative to any of our melt compositions.

Discussion

Effect of alkalis

Our results show clearly that alkalis have a positive effect on CO_2 solubility in basaltic melts as shown by previous studies (e.g., Dixon 1997; Behrens et al. 2009).

At any investigated pressure, the tephrite from Vesuvius dissolves 1.4 more CO_2 than the Etnean basalt, and 1.7 more CO_2 than the Strombolian basalt, and up to 2 times more CO_2 than a MORB (Dixon et al., 1995). This general trend is confirmed and extended by the data of Behrens et al. (2009). This effect is illustrated in figure 4: for each isobar, there exists a positive relationship between CO_2 solubility and the alkalinity of the melt.

These results were obtained using the same extinction coefficients for the three basaltic compositions. If we consider now different extinction coefficients for our three basaltic melt compositions, using the method of Dixon and Pan (1995), we obtain similar results to those obtained with the molar extinction coefficient of Fine and Stolper (1986) for VES-9 (2% lower) and PST-9 (2% higher). Only for ETN-1 are the results obtained with the Dixon and Pan method different, compared to those obtained with the constant extinction coefficient. This is simply explained by the fact that Dixon and Pan (1995) method takes into account of the Ca and Na contents, the concentration in the latter element being higher in the Etnean composition relative to the two other basaltic compositions. However, regardless of which extinction coefficient is used (constant or specific to each composition), the same effect of alkalis is observed with pressure: VES-9 dissolves more CO_2 than ETN-1 and then than PST-9. We thus conclude that alkalis (Na_2O+K_2O) have broadly a positive effect on the CO_2 solubility in basaltic melts (see also King and Holloway, 2002). In the following, we consider the CO_2 solubility results obtained by using the molar extinction coefficient of by Fine and Stolper (1986).

Refinement of the model of Dixon (1997)

Dixon (1997) used experimentally measured solubilities of CO_2 in alkali basalts (composition from a MORB to a leucitite) to propose a method to rationalise the influence of melt

composition on CO_2 solubility. Dixon (1997) defined a compositional parameter Π which takes into account the roles of Si^{4+}, Al^{3+}, Ca^{2+}, K^+, Na^+, Mg^{2+} and Fe^{2+} cation fractions:

$$\Pi = -6.50(Si^{+4} + Al^{+3}) + 20.17(Ca^{+2} + 0.8K^{+1} + 0.7Na^{+1} + 0.4Mg^{+2} + 0.4Fe^{+2}) \quad (19)$$

With this factor, the solubility of CO_2 in alkali-rich basalts can be predicted at 1200°C and 1000 bars. CO_2 solubilities for our three compositions at 1200°C and 1000 bars are plotted against the factor Π and show a good agreement with the linear relationship predicted by Dixon (1997) (figure 6). Also represented is the composition of Behrens et al (2009), obtained from linear extrapolation to 1 kbar of the results obtained by these authors at 2 and 5 kbar (which yields at 1 kbar a CO_2 content of 767 ppm).

Overall, the available experimental data base supports the parameterisation between CO_2 solubility and the Π factor proposed by Dixon (1997) at 1200°C and 1000 bar as a useful tool for the description of CO_2 solubility in basalt melts of variable alkalinity. At 1 kbar and 1200°C, the extended data base yields the following equation:

$$CO_2 \text{ (ppm)} = 920 \ (\pm 1)\Pi - 17 \ (\pm 53), \quad R^2 = 0.89 \quad (20)$$

CO_2 solubilities at 1000 bars calculated with equation (20) are slightly lower (<10%) than the CO_2 solubilities calculated by using the former regression coefficients of Dixon (1997). Calculating the CO_2 solubility with the new regression, and comparing to actual CO_2 contents, differences are less than 15% for both VES-9 and PST-9, whilst for the Etna composition the back calculated values may differ by up to 30%. Despite such an uncertainty equation (20) can be used to predict to a first approximation the CO_2 solubility of basaltic magmas of different alkali contents at 1 kbar and 1200°C. Although there are not enough data to test its validity at pressures other than 1 kb, we can only assume that such a correlation holds true up to 2 kbar.

Thermodynamic model

In this section we address the thermodynamics of CO_2 solution in our basaltic melts, using essentially the same approach as Dixon et al. (1995). Recent work on CO_2 solubility on a variety of silicate melts have emphasized that the anhydrous major element composition has relatively little effect on CO_2 solubility up to 2 kbar (Botcharnikov et al., 2005; 2006). In contrast, it has been shown that dissolution of water may profoundly affect the CO_2 solubility trends in a variety of silicate liquids (Mysen, 1976), the case being made strongly for andesitic to dacitic compositions (Jakobsson, 1997; King and Holloway, 2002; Behrens et al., 2004; Botcharnikov et al., 2005). In particular, experiments show that water presence

enhances the solubility of CO_2, leading to strong departure from Henrian behaviour, notably at high pressures (>2 kb), in agreement with earlier suggestion by Mysen (1976). Owing to water production upon reduction of ferric/ferrous iron, none of our melts is anhydrous, which means that we lack the benchmark needed to evaluate whether introduction of water in our basaltic melts indeed affects their CO_2 solubility in the investigated pressure range. However, Behrens et al. (2009) observed a near linear relationships between dissolved CO_2 and XCO_2 at 2 kbar for their phonotephrite composition, suggesting small departure from Henrian behaviour at this, and presumably below it, pressure. Similarly, the work of Dixon et al. (1995) investigated pressures below 1 kb, and noted an essentially Henrian behaviour of CO_2 solubility, despite that the water content of their quenched melts was in the range 1-2 wt%, as in our charges. Comparison with their data, obtained by equilibrating a MORB melt with an CO_2-H_2O vapour, with those of Stolper and Holloway (1988) and Jendrzejewsky et al. (1997), which were obtained under drier conditions (H_2O<0.6 wt%) than ours, shows that all data sets fall on the same fCO_2 vs CO_2^{melt} trend. This indicates that the presence of 1-2 wt% H_2O does not affect significantly the systematics of CO_2 solubility in basaltic melts up to an fCO_2=3000 bar at least, which is the maximum fCO_2 reached in our experiments, or that such an effect is not detectable with the analytical tools used to determine dissolved CO_2. In contrast, the few data available at 5 kb for basalts equilibrated with mixed H_2O-CO_2 fluids show a significant departure from linear behaviour between dissolved CO_2 and fCO_2 (Botcharnikov et al., 2005; Behrens et al., 2009), which has been interpreted as resulting from the depolymerising effects of OH- groups which enhances CO_2 solubility (Mysen, 1976, see also Behrens et al. 2009).

In view of the above, we have modelled our experimental data using the same approach as Dixon et al. (1995), keeping in mind that our model is essentially calibrated on hydrous basalts with dissolved water contents up to 2 wt% at pressures below 3 kb. Application of the equations derived below to wetter melts may result in overestimated pressures of fluid saturation.

The solubility of carbon dioxide in basaltic liquids can be described by the following simple reaction (e.g. Stolper and Holloway, 1988):

$$CO_{2,mol_{(v)}} + O^{2-}{}_{(m)} = CO_3^{2-}{}_{(m)} \qquad (21),$$
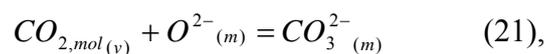
where $O^{2-}{}_{(m)}$ represents any reactive oxygen species, $CO_{2,mol_{(v)}}$ is the molecular carbon dioxide in the vapor phase, and $CO_3^{2-}{}_{(m)}$ is the carbonate groups dissolved in the melt. The equilibrium constant at T and P is equal to:

$$K(P,T) = \frac{a^m_{CO_3^{2-}}(P,T)}{a^m_{O^{2-}} * f_{CO_2}(P,T)} \qquad (22).$$

Assuming that $O^{2-}_{(m)}$ and $CO_3^{2-}_{(m)}$ mix ideally (Stolper et al., 1997), the activity of the melt species can be substituted by their mole fractions, so that:

$$K(P,T) = \frac{X^m_{CO_3^{2-}}(P,T)}{X^m_{O^{2-}} * f_{CO_2}(P,T)} \qquad (23).$$

Then, standard thermodynamic manipulations (e.g., Holloway and Blank, 1994) show that the pressure and temperature effects on K are given by:

$$K(P,T) = K_0(P_0,T_0) \times \exp\left\{ -\int_{P_0}^{P} \frac{\Delta V_r^{0,m}}{RT} dP + \int_{T_0}^{T} \frac{\Delta H_{H_2O}^0(T,P_0)}{RT?} dT \right\} \qquad (24),$$

where $K_0(P_0,T_0)$ is the equilibrium constant at $P_0 = 1000$ bar and $T_0 = 1200°C$ the reference pressure and temperature, $\Delta V_r^{0,m}$ is the volume change of the condensed components of reaction 15:

$$\Delta V_r^{o,m} = \left(V_{CO_3^{2-}}^{o,m} \right) - \left(V_{O^{2-}}^{o,m} \right) \qquad (25),$$

where $\left(V_{CO_3^{2-}}^{o,m} \right)$ and $\left(V_{O^{2-}}^{o,m} \right)$ are the molar volume of species of the melt in their standard states. $\Delta H_{H_2O}^0$ is the heat of solution of a mole of CO_2 into the melt. Since we did not investigate specifically the temperature effect, an appropriate value of $\Delta H_{H_2O}^0$ (-13.1 kJ/mol) is that of basanite which has a composition intermediate between tholeiitic basalt and nephelinite (Holloway and Blank, 1994).

According to reaction 24, a plot of $\ln\left\{ \frac{f_{CO_2}^0}{X_{CO_{2,tot}}} \right\}$ versus $\frac{(P-P_0)}{RT}$ obtained from CO_2 solubility data of experiments at constant temperature, results in a straight line whose slope gives $\Delta V_r^{o,m}$ ($X_{CO_{2,tot}}$ is the mole fraction of total CO_2 contents dissolved in the melt; figure 7).

Values calculated for VES-9, PST-9 and ETN-1 are similar to values found in previous works (Table 4): from 21.5 cm³/mol for leucitite (Thibault and Holloway, 1994), to 28 cm³/mol for tholeiite (Stolper and Holloway, 1988). There is no clear dependence between $\Delta V_r^{o,m}$ and the Π parameter, however. Considering the assumptions and uncertainties associated to the determination of $\Delta V_r^{o,m}$ with the above method we can only say that in most basaltic liquids $\Delta V_r^{o,m}$ is close to 25±3 cm³/mol. It is also important to note that the values of $\Delta V_r^{o,m}$

calculated here are for moderately hydrous basalts only and should not be interpreted as an accurate measurement of $\Delta V_r^{o,m}$ (e.g., Zhang,1999).

Then, knowing values of $\Delta V_r^{o,m}$, values of $\ln K_0$ can be calculated. Values found are similar to those calculated in previous works (Table 4). The influence of melt composition on the solubility of CO_2 is borne out by the variability of $K°$ constants determined in this and other studies (Holloway and Blank, 1994). A plot of $\ln K°$ versus Π (Fig. 8) reveals that there exists a good linear relationship between these two parameters.

Linear regression of the data set yields the following equation:

$$\ln K° = 0.893 \, \Pi - 15.247 \qquad (26)$$

with a correlation coefficient $R^2 = 0.891$.

The above parameterisation of the $K°$ coefficient offers a simple model of calculating the solubility of CO_2 in basaltic melts with varying alkali contents. The results of back calculations of the CO_2 contents of our experimental quenched glasses performed with this model are shown against measured CO_2 values (Fig. 9). The model appears to retrieve observed CO_2 contents to within 10% relative.

Application to the calculation of saturation pressures for alkali-rich basaltic compositions

Having determined solubility the laws of H_2O (Lesne et al., this issue) and CO_2 in the three basaltic melts from Vesuvius, Etna and Stromboli, we are now able to calculate saturation pressures of melt inclusions analysed in related volcanic products. By determining the total water and CO_2 dissolved in the melt inclusions, we are able to calculate fugacities and partial pressures of those species, and then the saturation pressures at which volatiles were entrapped in the melt inclusion (ignoring the role of other volatiles, in particular sulphur and halogens).

For Vesuvius, we use the data of Marianelli et al. (1999, 2005) and Fulignati et al. (2004) to calculate saturation pressures. In those previous works, the quantities of dissolved water and carbon dioxide were determined via FTIR measurements. They considered the OH stretching vibration band at 3535 cm-1 for measuring the water content, which was not used for measuring water content in our experimental glasses. CO_2 contents were calculated using the Dixon and Pan (1995) relationship (Marianelli et al., 2005) and using ε_{1515} =365 l.mol-1.cm-1 (Fulignati et al., 2004) and ε_{1515} = 380 l.mol-1.cm-1 (Cioni, 2000). Those values of ε_{1515} are not so different from that of Fine and Stolper (1986) used in this study, and translate into a maximum difference of 3% on the total carbon dissolved in the melt. Such a difference in CO_2 content will not induce a significant effect on the saturation pressures calculated. Both

Marianelli et al. (1999, 2005) and Fulignati et al. (2004) used VolatileCalc to calculate saturation pressures. Comparison of their findings with our own model shows that previous calculated pressures were overestimated by 50% on average (figure 10a).

For Etna we use the recent data of Métrich et al. (2004) and Spilliaert et al. (2006) who calculated saturation pressures with the VolatileCalc model (Newman and Lowenstern, 2002). To determine the CO_2 content of melt inclusions, Spilliaert et al. (2006) used a LPS nuclear microprobe, whilst for water they used a CAMECA IMS3f ion microprobe. Métrich et al. (2004) determined, instead, water and carbon contents by using the FTIR technique. As for Vesuvius, Métrich et al. (2004) determined water contents by using the total water band assignment and determined CO_2 content by using the molar extinction coefficient calculated from the Dixon and Pan (1995) relationship. Thus, CO_2 contents in melt inclusions and in our glasses are comparable, whereas the method used to calculate water content is not the same which could induce some differences in calculated water fugacities. Our calculated range of saturation pressures varies from 200 to 4200 bars, which is broadly similar to the range of pressures calculated by Métrich et al. (2004) and Spilliaert et al. (2006) (figure 10b).

For Stromboli, we refer to the data of Métrich et al. (2001) and Bertagnini et al. (2003) who calculated saturation pressures of melt inclusions by using Papale's (1999) model. Both determined water and total carbon contents in the melt inclusions by using FTIR and the relationship of Dixon and Pan (1995) to determine ε_{1515}. Métrich et al. (2001) used extinction coefficient values for the 5200 and 4500 cm-1 band assignments of Dixon et al. (1995), whereas Bertagnini et al. (2003) used the 3535 cm-1 band assignment. Thus, the data of Métrich et al. (2001) are directly comparable to ours, contrary to the water contents of Bertagnini et al. (2003). However, as CO_2 largely predominates over H_2O when calculating saturation pressures, comparison between our calculations and those of previous works can still be done faithfully. Métrich et al. (2001) and Bertagnini et al. (2003) found a range of saturation pressures from 2800 up to more than 4000 bars, with a cluster at 3500 bars. Both studies do not tabulate the calculated pressures, which prevents us from drawing a comparative plot such as done for Vesuvius and Etna. Our results yield a range of saturation pressures from 1500 to 3000 bars, with a cluster at 2500 bars, which is 1000 bars less than the cluster found by Bertagnini et al. (2003).

It thus appears that VolatileCalc overestimates the saturation pressures by 70% for Vesuvius basalt, by 26% for Stromboli and by 14% for Etnean basalt. Botcharnikov et al (2005) have already shown that VolatileCalc does not work properly at pressures significantly higher than 2 kb, tending also to overestimate fluid saturation pressures for common basalt-

andesite-rhyolite melts. The present study shows that a further limitation of this model is its failure in correctly predicting saturation pressures for alkali-rich mafic melts. A similar conclusion was reached by Behrens et al. (2009). For those melts, it appears that more complex models, such as that of Papale (1999), are needed to better account for the possible interactions between H_2O and CO_2 in silicate melts (see for instance Tamic et al., 2001), in addition to other compositional effects.

Conclusions

Experiments at 1200°C and pressures from 250 to 2086 bar have been performed to determine the solubilities of CO_2 in alkali basaltic melts.

1. Results of CO_2 contents presented in this study were measured by infrared measurements. Without any bulk carbon data, we used the molar extinction coefficient given by Fine and Stolper (1986) for basaltic melts, as well as molar extinction coefficients calculated from the melt composition given by Dixon and Pan (1995). Clearly, there is still a large uncertainty surrounding the determination of extinction coefficients in basaltic glasses and their variations with alkali and alkali-earth elements, which considerably hamper an accurate determination of dissolved CO_2 in basalts other than MORBs. Future work should be directed at a better definition of such a relationships

2. Aside from this problem, our experiments, along with previous similar works, show that the solubility of any particular melt can be modelled in a simple way. For the three worked compositions, such simple relationships are:

$$f_{CO_2}^{1200°C} = 8.57*10^6 * X_{CO_2}^m {}^{1.26}; \qquad R^2 = 0.99 \text{ for Vesuvius} \qquad (27)$$

$$f_{CO_2}^{1200°C} = 1.14*10^7 * X_{CO_2}^m {}^{1.23}; \qquad R^2 = 0.93 \text{ for Etna} \qquad (28)$$

$$f_{CO_2}^{1200°C} = 3.49*10^6 * X_{CO_2}^m {}^{1.04}; \qquad R^2 = 0.99 \text{ for Stromboli} \qquad (29).$$

3. Experimental results obtained on these basaltic compositions show a strong effect of alkalis on CO_2 behaviour in these melts, confirming previous studies (Dixon, 1997; Behrens et al., 2009): at any pressure of the investigated range, alkali-rich basalts dissolve up to 1.7 times more CO_2 than alkali-poor basalts, and up to 2 times more than a MORB.

4. Data obtained in this study provide a refinement of the model of Dixon (1997): the parameterisation between the CO_2 solubility at 1 kbar and 1200°C and the Π factor is confirmed, and the extended data base yields: CO_2 (ppm) = 920 (±1)Π - 17 (±53),

5. Comparing our data with those obtained in previous works, it appears that there exists a compositional dependence for $\ln K°$, which varies linearly with the Π parameter, therefore providing a basis for a simple thermodynamical modelling of CO_2 solubility in basaltic melts.

6. Lastly, application of our results to the calculation of volatile saturation pressures using dissolved H_2O and CO_2 contents of primitive melt inclusions from the three studied volcanoes shows that previous saturation pressures of primitive magmas feeding these volcanoes were significantly overstimated, notably for the Vesuvius.

References

Behrens H, Ohlhorst S, Holtz F, Champenois M (2004) CO2 solubility in dacitic melts equilibrated with H_2O-CO_2 fluids: Implications for modelling the solubility of CO_2 in silicic melts. Geochimica et Cosmochimica Acta 68: 4687-4703

Behrens H, Misiti V, Freda C, Vetere F, Botcharnikov RE and Scarlato P (2009) Solubility of H_2O and CO_2 in ultrapotassic melts at 1200 and 1250 degrees C and pressure from 50 to 500 MPa. American Mineralogist 94:105 -120

Berndt J, Liebske C, Holtz F, Freise M, Nowak M, Ziegenbein D, Hurkuck W, Koepke J (2002) A combined rapid-quench and H-2-membrane setup for internally heated pressure vessels: Description and application for water solubility in basaltic melts. American Mineralogist 87:1717-1726

Bertagnini A, Metrich N, Landi P, Rosi M (2003) Stromboli volcano (Aeolian Archipelago, Italy): An open window on the deep-feeding system of a steady state basaltic volcano. Journal of Geophysical Research-Solid Earth 108(B7) doi:10.1029/2002JB002146

Blank JG, Stolper EM, Carroll MR (1993) Solubilities of carbon-dioxide and water in rhyolitic melt at 850 degrees C and 750 bars. Earth and Planetary Science Letters 119(1-2):27-36

Blank JG, Brooker RA (1994) Experimental studies of carbon-dioxide in silicate melts. Solubility, speciation, and stable carbon-isotope behaviour. In: Volatiles in Magmas, vol 30. Mineralogical Soc America, Washington, pp 157-186

Botcharnikov R, Freise M, Holtz F, Behrens H (2005) Solubility of C-O-H mixtures in natural melts: new experimental data and application range of recent models. Annals of Geophysics 48:633-646

Botcharnikov RE, Behrens H, Holtz F (2006) Solubility and speciation of C-O-H fluids in andesitic melt at T=1100-1300 degrees C and P=200 and 500MPa. Chemical Geology 229: 125-143

Bourgue E, Richet P (2001) The effects of dissolved CO_2 on the density and viscosity of silicate melts: a preliminary study. Earth and Planetary Science Letters 193(1-2): 57-68

Burgisser A, Scaillet B (2007) Redox evolution of a degassing magma rising to the surface. Nature 445(7124): 194-197

Cioni R (2000) Volatile content and degassing processes in the AD 79 magma chamber at Vesuvius (Italy). Contributions to Mineralogy and Petrology 140(1): 40-54

Di Carlo I, Pichavant M, Rotolo SG, Scaillet B (2006) Experimental crystallization of a high-K arc basalt: The golden pumice, Stromboli volcano (Italy). Journal of Petrology 47(7): 1317-1343

Dixon JE, Pan V (1995) Determination of the molar absorptivity of dissolved carbonate in basanitic glass. American Mineralogist 80: 1339-1342

Dixon JE, Stolper EM, Holloway JR (1995) An experimental study of water and carbon dioxide solubilities in mid ocean ridge basaltic liquids .1. Calibration and solubility models. Journal of Petrology 36: 1607-1631

Dixon JE (1997) Degassing of alkalic basalts. American Mineralogist 82: 368-378

Ferry JM and Baumgartner L (1987) Thermodynamic models of molecular fluids at the elevated pressures and temperatures of crustal metamorphism (1987) Reviews in Mineralogy 17: 323-365

Fine G, Stolper E (1985) The speciation of carbon-dioxide in sodium aluminosilicate glasses. Contributions to Mineralogy and Petrology 91(2): 105-121

Fine G, Stolper E (1986) Dissolved carbon-dioxide in basaltic glasses. Concentrations and speciation. Earth and Planetary Science Letters 76(3-4): 263-278

Fulignati P, Marianelli P, Metrich N, Santacroce R, Sbrana A (2004) Towards a reconstruction of the magmatic feeding system of the 1944 eruption of Mt Vesuvius. Journal of Volcanology and Geothermal Research 133(1-4): 13-22

Holloway JR, Blank JG (1994) Application of experimental results to C-O-H species in natural melts. In: Volatiles in Magmas, vol 30. Mineralogical Soc America, Washington, pp 187-230

Holloway JR, Pan V, Gudmundsson G, Hb (1992) High-pressure fluid-absent melting experiments in the presence of graphite: oxygen fugacity, ferric/ferrous ration and dissolved CO_2. European Journal of Mineralogy 4: 105-114

Holloway JR (1987) Igneous fluids. Reviews in Mineralogy 17: 211-233

Holloway JR (1977) Fugacity and activity of molecular species in supercritical fluids. Thermodynamics in Geology: 161-181

Jakobsson S (1997) Solubility of water and carbon dioxide in an icelandite at 1400 degrees C and 10 kilobars. Contributions To Mineralogy And Petrology 127: 129-135

Jendrzejewski N, Trull TW, Pineau F, Javoy M, Xa (1997) Carbon solubility in Mid-Ocean Ridge basaltic melt at low pressures (250-1950 bar). Chemical Geology 138(1-2): 81-92

King PL, Holloway JR (2002) CO_2 solubility and speciation in intermediate (andesitic) melts: The role of H_2O and composition. Geochimica Et Cosmochimica Acta 66: 1627-1640

Lange RA (1994) The effect of H_2O, CO_2 and F on the density and viscosity of silicate melts. In: Volatiles in Magmas, vol 30. Mineralogical Soc America, Washington, pp 331-369

Lesne P, Scaillet B, Pichavant M, Iacono-Marziano G, Beny JM (in prep.) The H_2O solubility of alkali basalts: an experimental study

Marianelli P, Metrich N, Santacroce R, Sbrana A (1995) Mafic magma batches at Vesuvius. A glass inclusion approach to the modalities of feeding stratovolcanoes. Contributions to Mineralogy and Petrology 120(2): 159-169

Marianelli P, Metrich N, Sbrana A (1999) Shallow and deep reservoirs involved in magma supply of the 1944 eruption of Vesuvius. Bulletin of Volcanology 61(1-2): 48-63

Marianelli P, Sbrana A, Metrich N, Cecchetti A (2005) The deep feeding system of Vesuvius involved in recent violent strombolian eruptions. Geophysical Research Letters 32: L02306

Metrich N, Allard P, Spilliaert N, Andronico D, Burton M (2004) 2001 flank eruption of the alkali- and volatile-rich primitive basalt responsible for Mount Etna's evolution in the last three decades. Earth and Planetary Science Letters 228(1-2): 1-17

Metrich N, Bertagnini A, Landi P, Rosi M (2001) Crystallization driven by decompression and water loss at Stromboli volcano (Aeolian Islands, Italy). Journal of Petrology 42(8): 1471-1490

Morizet Y, Brooker RA, Kohn SC (2002) CO2 in haplo-phonolite Melt: Solubility, speciation and carbonate complexation. Geochimica et Cosmochimica Acta 66(10): 1809-1820

Mysen BO (1976) Experimental-determination of some geochemical parameters relating to conditions of equilibration of peridotite in upper mantle. American Mineralogist 61: 677-683

Newman S, Lowenstern JB (2002) VOLATILECALC: a silicate melt-H_2O-CO_2 solution model written in Visual Basic for excel. Computers & Geosciences 28(5): 597-604

Ohmoto H and Kerrick D (1977) Devolatilization equilibria in graphitic systems. American Journal of Science, 277: 1013-1044

Pan V, Holloway JR, Hervig RL (1991) The pressure and temperature-dependence of carbon-dioxide solubility in tholeiitic basalt melts. Geochimica Et Cosmochimica Acta 55(6): 1587-1595

Papale P (1997) Modelling of the solubility of a one-component H_2O or CO_2 fluid in silicate liquids. Contributions to Mineralogy and Petrology 126(3): 237-251

Papale P (1999) Strain-induced magma fragmentation in explosive eruptions. Nature 397(6718): 425-428

Papale P, Moretti R, Barbato D (2006) The compositional dependence of the saturation surface of H2O+CO2 fluids in silicate melts. Chemical Geology 229(1-3): 78-95

Pawley AR, Holloway JR, McMillan PF (1992) The effect of oxygen fugacity on the solubility of carbon oxygen fluids in basaltic melt. Earth and Planetary Science Letters 110(1-4): 213-225

Pichavant M, Di Carlo I, Le Gac Y, Rotolo S, Scaillet B (2009) The deep feeding system of basaltic volcanoes: experimental evidence from Stromboli (Italy). Journal of Petrology 50: 601-624

Richet P, Whittington A, Holtz F, Behrens H, Ohlhorst S, Wilke M, (2000) Water and the density of silicate glasses. Contributions to Mineralogy and Petrology 138: 337-347

Robock A (2000) Volcanic eruptions and climate. Reviews of Geophysics 38(2): 191-219

Roux J, Lefevre A (1992) A fast-quench device for internally heated pressure-vessels. European Journal of Mineralogy 4: 279-281

Silver L, Stolper E (1985) A thermodynamical model for hydrous silicate melts. Journal of Geology 93: 161-177

Spilliaert N, Allard P, Metrich N, Sobolev AV (2006a) Melt inclusion record of the conditions of ascent, degassing, and extrusion of volatile-rich alkali basalt during the powerful 2002 flank eruption of Mount Etna (Italy). Journal of Geophysical Research-Solid Earth 111: B04203

Spilliaert N, Metrich N, Allard P (2006b) S-Cl-F degassing pattern of water-rich alkali basalt: Modelling and relationship with eruption styles on Mount Etna volcano. Earth and Planetary Science Letters 248(3-4): 772-786

Stolper E, Fine G, Johnson T, Newman S (1987) Solubility of carbon-dioxide in albitic melt. American Mineralogist 72: 1071-1085

Stolper E, Holloway JR (1988) Experimental determination of the solubility of carbon-dioxide in molten basalt at low-pressure. Earth and Planetary Science Letters 87(4): 397-408

Thibault Y, Holloway JR, Na (1994) Solubility of CO_2 in a Ca-rich leucitite. Effects of pressure, temperature, and oxygen fugacity. Contributions to Mineralogy and Petrology 116(1-2): 216-224

Zhang Y (1999) H_2O in rhyolitic glasses and melts: Measurement, speciation, solubility, and diffusion. Reviews of Geophysics, 37: 493–516
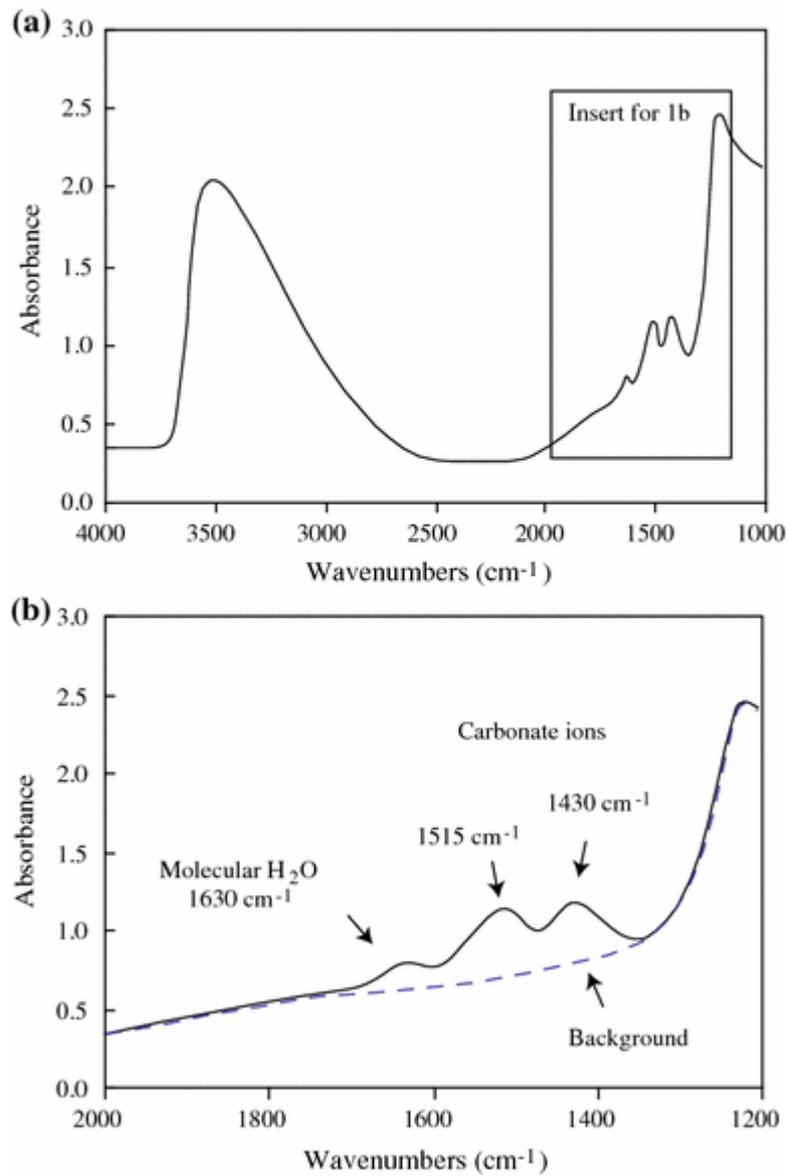
Figure 1:

Typical mid-IR spectrum of basaltic glass from experiment run1#4 (ETN-1) (thickness 133µm) showing the absorptions of carbonate bands (1515 cm-1 and 1430 cm-1). Small peaks at 2350 cm-1 are absorptions by atmospheric CO_2. Background modelled as described in text.
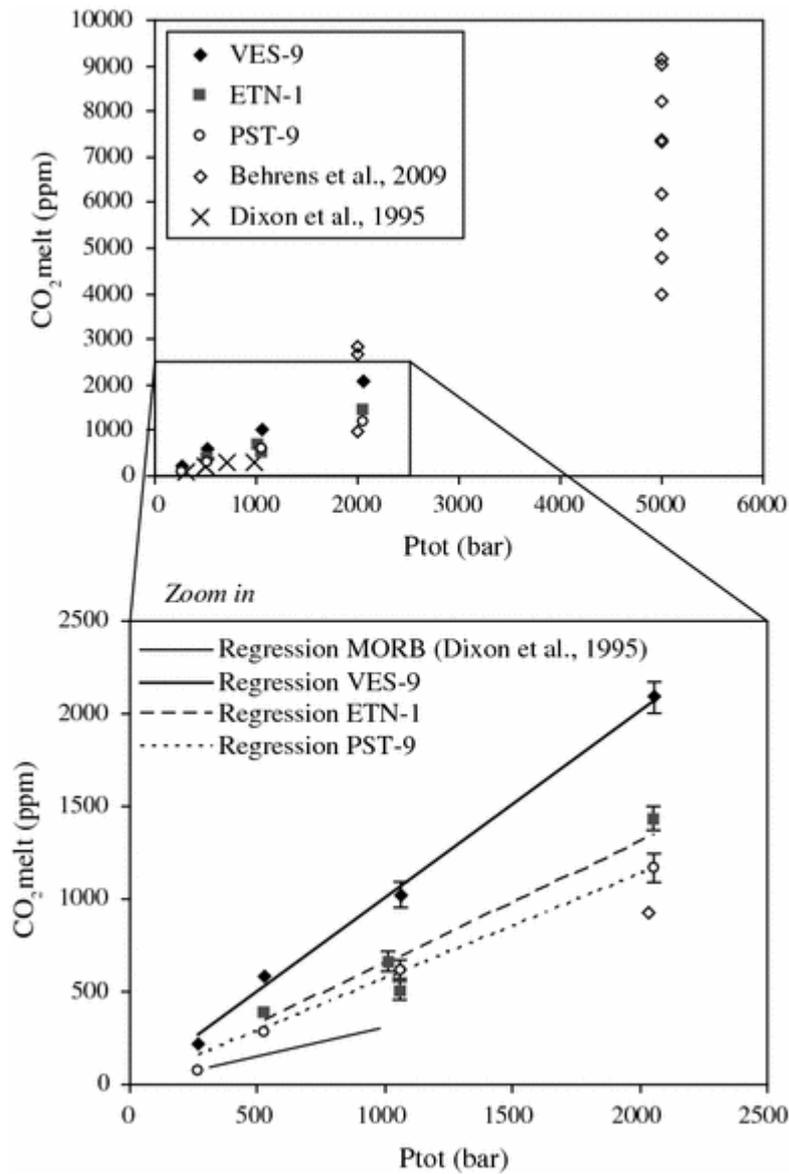
Figure2:

Experimental results on CO_2 contents in basaltic melts (Vesuvius, Etna, Stromboli and MORB from Dixon et al., 1995), versus experimental pressure.
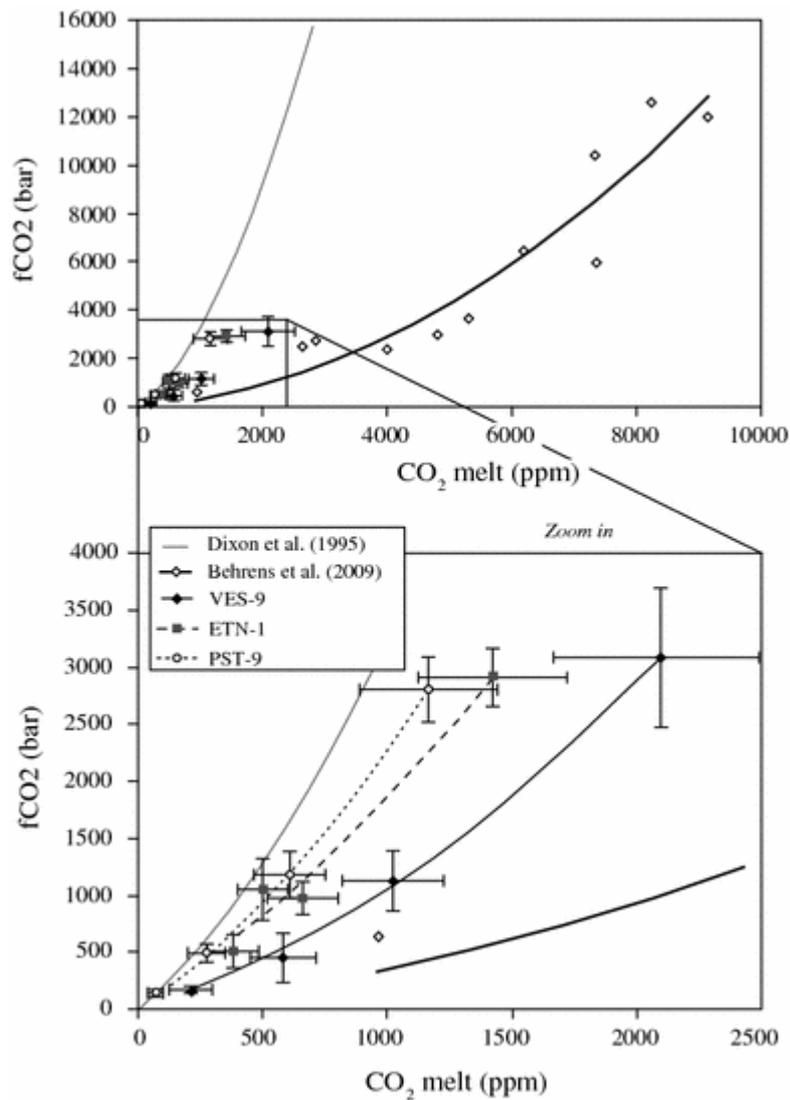
Figure 3:

Fugacity of CO_2 for VES-9, ETN-1 and PST-9, calculated with an MRK equation of state (Holloway, 1977), versus CO_2 dissolved in the melts in ppm. Model from Dixon et al. (1995) obtained on MORB are reported. Errors on f_{CO2} are smaller than the symbols.
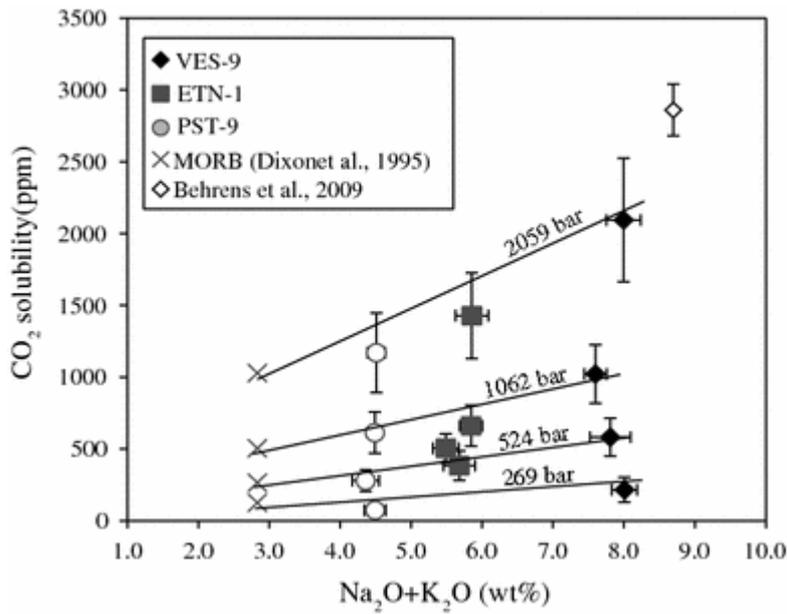
Figure 4:

CO_2 solubility calculated at experimental pressures in basaltic melts against the alkalinity of the melt.
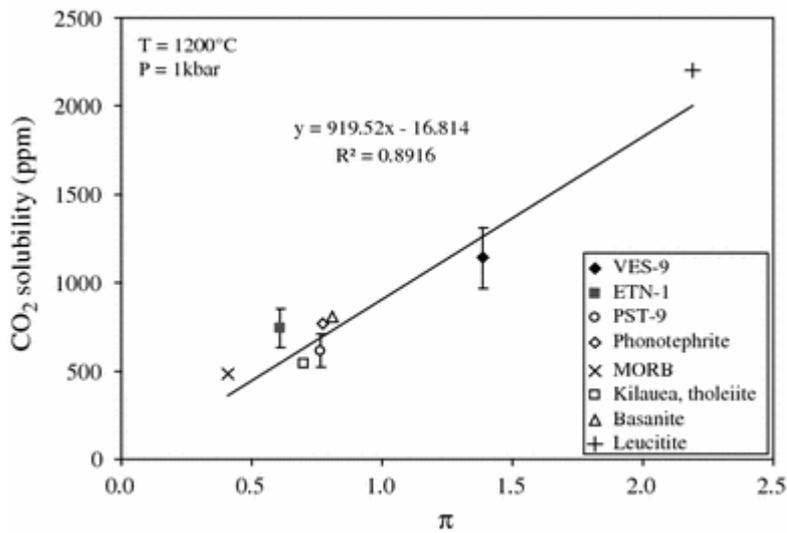
Figure 5:

Saturation pressures calculated with VolatileCalc (Newmann and Lowenstern, 2002) for VES-9, ETN-1, PST-9, taking total SiO_2 measured in hydrous glass, at T = 1200°C, versus experimental pressures. Calculated saturation pressures of MORB (Dixon et al., 1995) were calculated and reported (crosses).
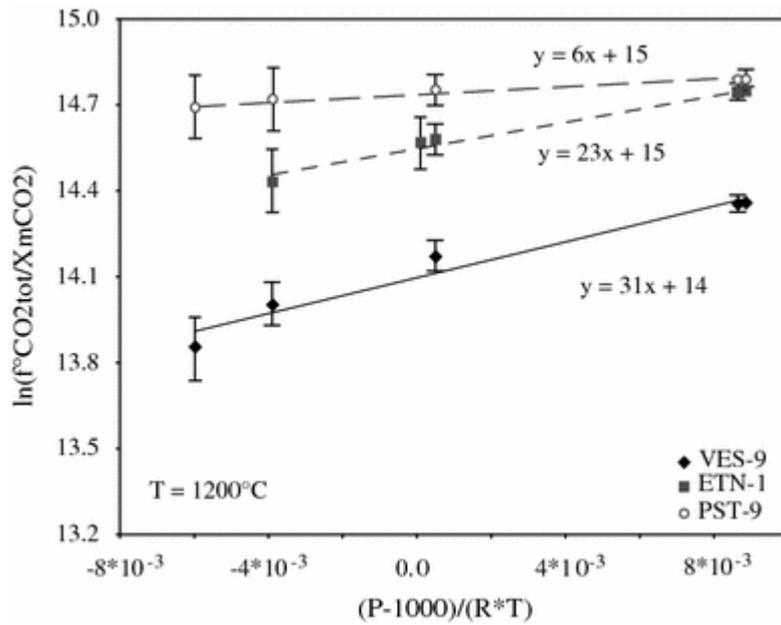
Figure 6:

CO_2 (ppm) solubility calculated for Vesuvius, Etna and Stromboli at 1200°C and 1 kbar, using solubility laws defined in this study, against the Π factor defined by Dixon (1997).
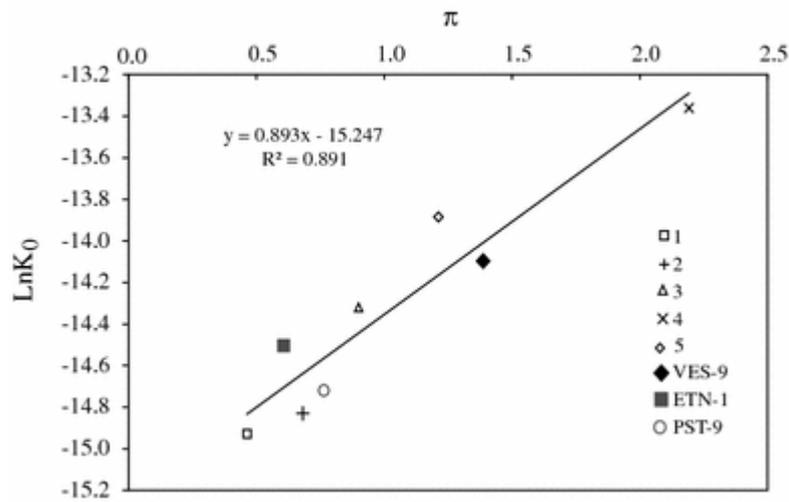
Figure 7:

Determination of $\Delta V_r^{o,m}$ by fitting $\ln\left\{\dfrac{f_{CO_2}^0}{X_{CO_{2,tot}}}\right\}$ versus $\dfrac{(P-P_0)}{RT}$.
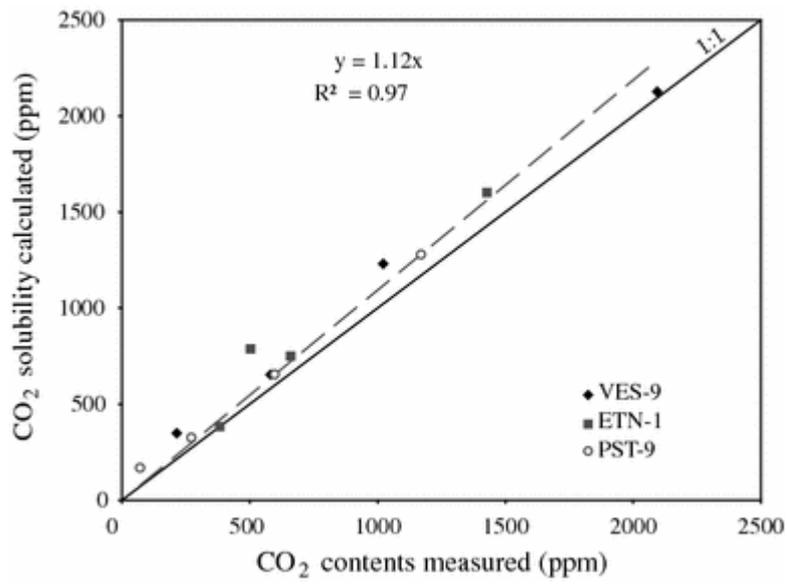
Figure 8:

LnK° versus Π parameter (Dixon 1997).
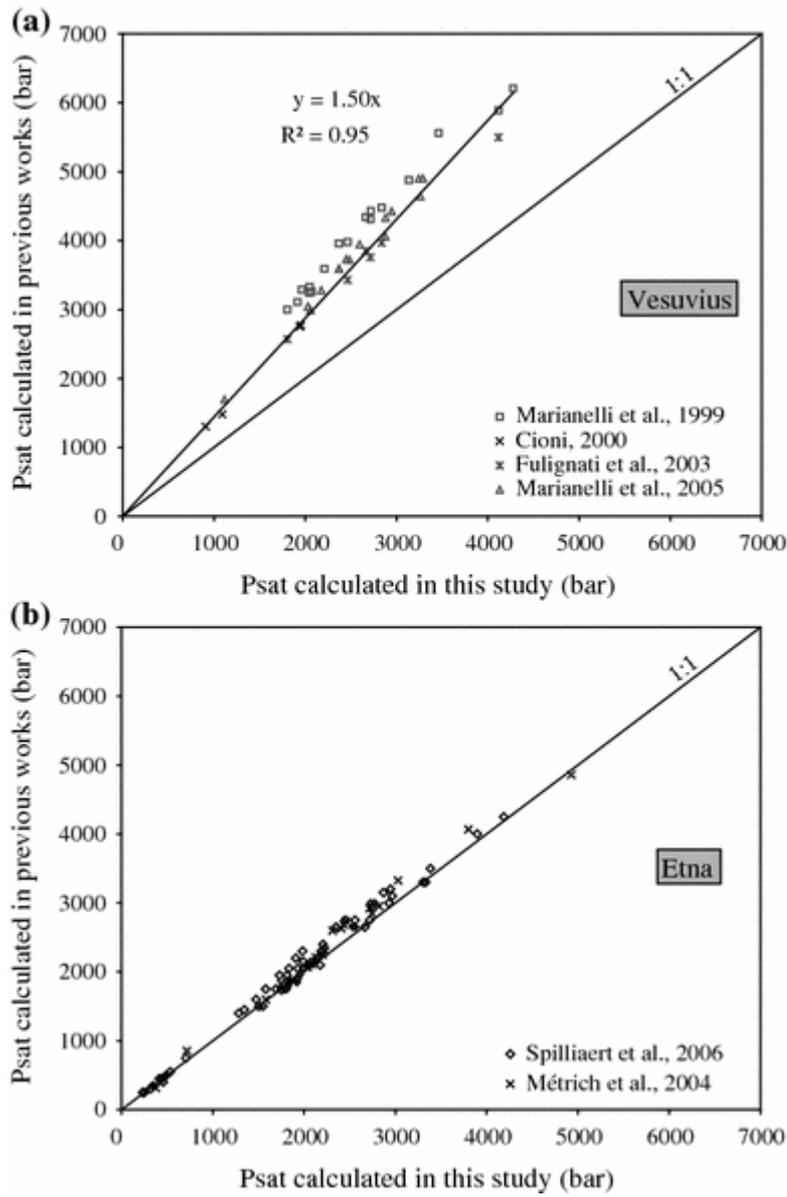
Figure 9:

Comparison between measured and calculated CO_2 content with the thermodynamical parameters calculated in this study.
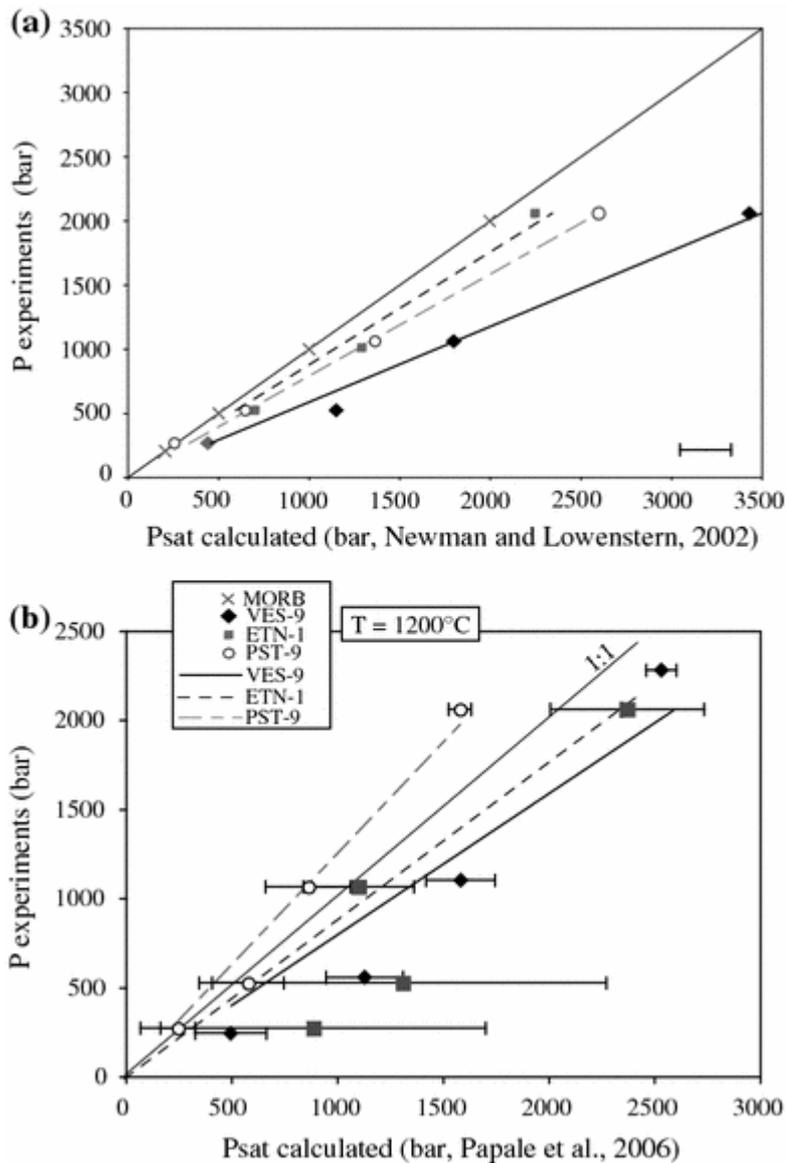
Figure 10:

Saturation pressures calculated by using data from melt inclusions of (a) Vesuvian products from Marianelli et al (1999), Cioni (2000), Fulignati et al. (2004) and Marianelli (2005) and of (b) Etnean products Métrich et al. (2004) and Spilliaert et al. (2006), compared to the saturation pressures calculated by using our solubility laws.

Tables

Table 1 Bulk rock compositions

Oxides	VES-9[a]	ETN-1[b]	PST-9[c]
SiO_2	48.67	47.95	49.82
TiO_2	0.97	1.67	0.81
Al_2O_3	14.72	17.32	15.94
FeO	7.62	10.24	7.71
MnO	0.14	0.17	0.20
MgO	6.82	5.76	8.07
CaO	12.94	10.93	12.81
Na_2O	1.82	3.45	2.32
K_2O	5.63	1.99	1.92
P_2O_5	0.66	0.51	0.40
Total	100.00	100.00	100.00

[a]Natural alkali basalt from VES-9
[b]Natural alkali basalt from ETN-1
[c]Natural alkali basalt from PST-9

Table 2 Experimental conditions and FTIR results for H_2O and CO_2 dissolved in experimental glasses

Run	Composition	Capsule	wt% H_2O loaded	wt% CO_2 loaded	% FeO kept [a]	wt% H_2O_{tot} [b]	CO_2 [c] (ppm)	CO_2 [d] (ppm)
Experiment 1: 2,059 bars, duration: 4 h								
Run1#2	VES-9	Pt	0	3.93	68	0.80 ± 0.40	2,094 ± 431	2,061 ± 431
Run1#4	ETN-1	Pt	0	4.15	79	1.49 ± 0.13	1,429 ± 299	1,638 ± 299
Run1#6	PST-9	Pt	0	4.35	70	1.58 ± 0.16	1,170 ± 277	1,196 ± 277
Experiment 2: 1,013 bars, duration: 8 h								
Run2#8	ETN-1	Pt	0	1.91	70	1.55 ± 0.23	661 ± 142	757 ± 142
Experiment 3: 524 bars, duration: 4 h								
Run3#4	VES-9	Pt	0	3.93	83	0.82 ± 0.37	582 ± 132	572 ± 132
Run3#5	ETN-1	Pt	0	3.94	83	0.73 ± 0.20	383 ± 103	440 ± 103
Run3#6	PST-9	Pt	0	3.50	93	0.71 ± 0.10	279 ± 75	285 ± 75
Experiment 4: 269 bars, duration: 4 h								
Run4#4	VES-9	Pt	0	1.24	69	0.85 ± 0.08	215 ± 87	212 ± 87
Run4#5	ETN-1	Pt	0	1.57	81	0.95 ± 0.10	n.d.	n.d.
Run4#6	PST-9	Pt	0	1.00	72	0.98 ± 0.07	73 ± 31	75 ± 31
Experiment 19: 1,062 bars, duration: 5 h								
Run19#1	VES-9	Pt	0	3.16	74	1.02 ± 0.23	1,022 ± 204	1,006 ± 204
Run19#2	ETN-1	Pt	0	2.74	74	1.51 ± 0.39	504 ± 101	578 ± 101
Run19#3	PST-9	Pt	0	2.59	71	0.91 ± 0.15	613 ± 144	626 ± 144

[a] Proportion of FeO kept in the glass relative to the initial glass FeO concentration, calculated as $100*FeO_{glass}/FeO_{starting\ glass}$, with $FeO_{starting\ glass}$ from Table 1

[b] H_2O determined by NIR-FTIR measurements (see text for explanation)

^{c}CO$_2$ determined by MIR-FTIR measurements and calculated with Beer–Lambert law, using ε_{1515} from Fine and Stolper (*1986*)

^{d}CO$_2$ determined by MIR-FTIR measurements and calculated with Beer–Lambert law, using ε_{1515} from Dixon and Pan (*1995*)

Table 3 Experimental results obtained on basalt from (a) Vesuvius, (b) Etna and (c) Stromboli

P_{tot} (bar)	Run	Na$_2$O + K$_2$O	Density^a (g/l)	% FeO kept^b	wt% H$_2$O$_{mol}$ ^{c}	wt% OH^c	wt% H$_2$O$_{tot}$ ^{c}	CO$_2$ (ppm)^d	e	f	g	g	h	h	h	h	i
(a)																	
2,059	Run1#2	7.99	2,696	68.36	0.36	0.44	0.80	2,094	87	3,128	0.041	0.959	1.61	0.73	1.76	0.17	−5.991
		_0.24_	_3_		_0.07_	_0.01_	_0.16_	_431_	_17_	_612_	_0.008_						
524	Run3#4	7.81	2,692	83.10	0.27	0.55	0.82	582	91	482	0.174	0.826	1.65	0.55	2.20	0.05	−5.952
		_0.28_	_2_		_0.12_	_0.02_	_0.37_	_132_	_40_	_217_	_0.078_						
269	Run4#4	8.01	2,692	69.32	0.27	0.58	0.85	215	96	183	0.359	0.641	1.71	0.53	2.35	0.02	−5.903
		_0.18_	_1_		_0.02_	_0.04_	_0.08_	_87_	_9_	_30_	_0.048_						
1,062	Run19#1	7.60	2,689	73.71	0.36	0.66	1.02	1022	131	1,165	0.124	0.876	2.05	0.72	2.67	0.08	−5.634
		_0.16_	_2_		_0.07_	_0.06_	_0.23_	_204_	_29_	_265_	_0.028_						
(b)																	
2,059	Run1#4	5.86	2,680	79.40	0.69	0.81	1.49	1429	216	2,926	0.103	0.897	2.99	1.37	3.22	0.12	−5.198
		_0.23_	_1_		_0.06_	_0.02_	_0.13_	_299_	_19_	_256_	_0.009_						
1,013	Run2# 8	5.84	2,679	69.84	0.80	0.74	1.55	661	231	967	0.229	0.771	3.09	1.61	2.97	0.05	−5.141
		_0.16_	_2_		_0.10_	_0.06_	_0.23_	_142_	_34_	_145_	_0.034_						
524	Run3#5	5.68	2,694	82.50	0.34	0.38	0.73	383	58	519	0.111	0.889	1.47	0.69	1.55	0.03	−6.341
		_0.22_	_1_		_0.09_	_0.02_	_0.20_	_103_	_16_	_145_	_0.031_						
269	Run4#5	5.57	2,690	81.42	0.55	0.41	0.95	n.d.	95	183	0.356	0.644	1.92	1.10	1.64	n.d.	−5.909
		_0.18_	_1_		_0.04_	_0.03_	_0.10_		_10_	_31_	_0.051_						
1,062	Run19#2	5.49	2,679	73.92	0.74	0.77	1.51	504	222	1,050	0.210	0.790	3.03	1.48	3.09	0.04	−5.175
		_0.18_	_4_		_0.19_	_0.04_	_0.39_	_101_	_57_	_272_	_0.054_						
(c)																	
2,059	Run1#6	4.51	2,678	69.61	0.66	0.92	1.58	1,170	285	2,820	0.136	0.864	3.16	1.32	3.69	0.10	−4.959

P_{tot} (bar)	Run	Na$_2$O + K$_2$O	Density[a] (g/l)	% FeO kept[b]	wt% H$_2$O$_{mol}$ [c]	wt% OH[c]	wt% H$_2$O$_{tot}$ [c]	CO$_2$ (ppm)[d]	e	f	g	g	h	h	h	h	i
		0.12	*1*		*0.06*	*0.03*	*0.16*	*277*	*28*	*286*	*0.014*						
524	Run3#6	4.36	2,694	93.22	0.30	0.41	0.71	279	71	504	0.136	0.864	1.43	0.61	1.66	0.02	−6.165
		0.19	*1*		*0.04*	*0.01*	*0.10*	*75*	*10*	*81*	*0.021*						
269	Run4#6	4.49	2,689	71.69	0.32	0.66	0.98	73	124	152	0.465	0.535	1.98	0.65	2.65	0.01	−5.678
		0.15	*1*		*0.06*	*0.02*	*0.17*	*31*	*22*	*33*	*0.091*						
1,062	Run19#3	4.49	2,691	71.07	0.34	0.57	0.91	613	109	1,192	0.103	0.897	1.83	0.69	2.28	0.05	−5.791
		0.10	*0*		*0.05*	*0.04*	*0.15*	*144*	*18*	*205*	*0.018*						

Table 4 Best-fit thermodynamic parameters for Eq. 17

Composition	ΔV^0	$\ln K_0$	P_0 (bar)	T_0 (°C)
VES-9	31	-14.10 ± 0.03	1,000	1,200
ETN-1	23	-14.55 ± 0.00	1,000	1,200
PST-9	6	-14.74 ± 0.01	1,000	1,200

	V carbonate				
Thibault et al. (*1994*)	Leucitite	22			
Pan et al. (*1991*)	Tholeiite	23 ± 1.03	-14.83 ± 0.1	1,000	1,200
Stolper and Holloway (*1988*)	Tholeiite	33 ± 0.5	-15.15 ± 0.06	1,000	1,200
Stolper et al. (*1987*)	NaAlSi3O8	25			
Spera and Bergman (*1980*)	Andesite CA	34			
Spera and Bergman (*1980*)	Tholeiite K1921	33			
Spera and Bergman (*1980*)	Olivine Melilite OM1	23			